Proceedings of 20th International Congress on Acoustics, ICA 2010

23-27 August 2010, Sydney, Australia

Airfoil trailing edge noise reduction by the introduction of sawtooth and slitted trailing edge geometries

Mathieu Gruber, Mahdi Azarpeyvand and Phillip F. Joseph

Institute of Sound and Vibration Research, Southampton, United Kingdom

PACS: 43.28.-G, 43.28.JS, 43.28.RA

ABSTRACT

This paper compares the measurements of the trailing edge self noise reduction obtained using sawtooth and slit serrations on a NACA651210 airfoil. This work is relevant to reducing the noise from aircraft engines, aircraft wings and wind turbines. A detailed experimental study conducted in the ISVR's open-jet wind tunnel reveals noise reductions of up to 5 dB over a large frequency range by the introduction of these trailing edge designs. This paper presents the noise measurements for a range of jet speeds and sawtooth and slit geometries. The airfoil is at 5^o angle of attack and the boundary layer has been tripped so as to become turbulent. Measurements of the static pressure coefficient distribution along the chord of the airfoil are also reported. This is to allow the effects on lift to be assessed. Noise measurements for the sawtooth serrations are compared to the theory derived by Howe. Howe's theory is extended to include a series of slits and compared to experiments. It is shown theoretically that for a sawtooth profile high levels of noise reduction can be achieved, either when the serration wavelength λ is smaller than the boundary layer thickness δ or when the root-to-tip distance h is larger than δ. It is shown theoretically that the slit serrations are not an effective noise reduction treatment since the noise reduction asymptotes to zero at high frequencies. Experimental measurements of the noise reduction obtained using trailing edge sawtooth and slits are shown to be significantly less than that predicted. The noise is shown to increase at frequencies above some critical frequency, which is shown to depend only on $f_0\delta / U_c \approx 1$ and independent of serration geometry.

INTRODUCTION

Aircraft noise in the vicinity of communities close to airports is of great concern, causing stringent night time curfews to be imposed on aircraft movements in and out of airports. The noise produced during takeoff and cutback is dominated by the engine, particularly the jet and the fan, whilst during landing the noise is mainly produced by the airframe, the wing and the under carriage. One important noise mechanism that is relevant to all these sources is the interaction between boundary layer turbulence, which forms on the surface of the blades / wings, with the airfoil trailing edge.

It has long been recognised that airfoil trailing edge noise may be reduced by modifying the trailing edge geometry so that the efficiency by which vorticity is scattered into sound is reduced. In this paper we consider the reduction of this noise source through the introduction of trailing edge serrations. This approach has been shown by a number of researchers to provide significant theoretical (Howe [1, 2]) and experimental (Dassen *et al* [3], Oerlemans *et al* [4], Parchen *et al* [5] Gruber *et al* [6]) reductions in self-noise radiation. A short review of Howe's trailing edge noise prediction model is first presented for straight and sawtooth serrated edges. An extension of this model to slit serrations is also derived. The experimental setup and the trailing edge geometries used for the study of trailing edge noise are then described. The effects of trailing edge serrations on the static pressure distribution along the airfoil chord are also assessed. Finally, this paper aims at comparing the noise radiation predicted by Howe's theory for sawtooth serrated egdes [2] and by Howe's extended theory for slit serrations against experimental data.

HOWE'S TRAILING EDGE NOISE MODEL

Noise prediction model: general derivation

This section is concerned with the mathematical modelling of the noise radiation from serrated trailing edges. The modelling is based on Howe's derivation of the problem [2] and includes the following assumptions:

- Frozen turbulence convected past the trailing edge of a semi-infinite flat plate.
- The model has infinite span.
- The flow is of low Mach number.
- The Kutta condition is satisfied.
- No other extraneous noise sources are present.

Figures 1 and 2 show a sketch of the sawtooth and slitted serration trailing edges together with the coordinate systems used in the derivation.

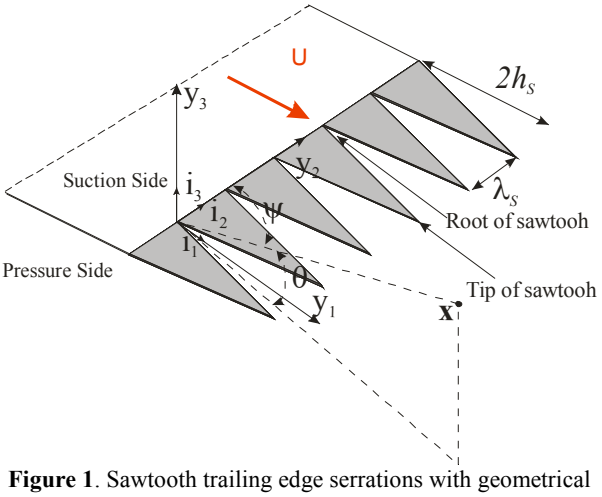

Figure 1. Sawtooth trailing edge serrations with geometrical parameters h and λ and definition of the coordinate system

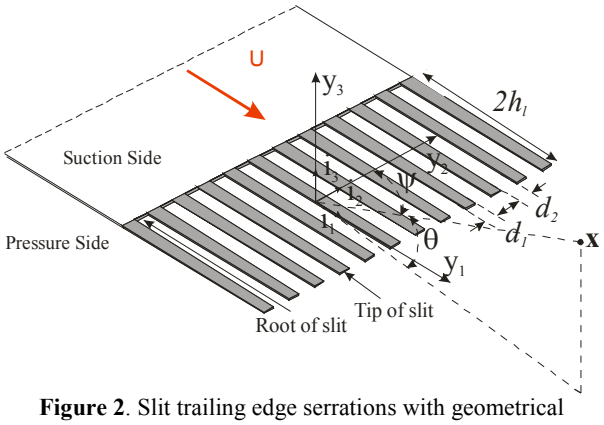

Figure 2. Slit trailing edge serrations with geometrical parameters d_1 and d_2 and definition of the coordinate system

The profiles of the geometries shown in Figures 1 and 2 are defined by $y_1 = \zeta(y_2)$. Equations (1) and (2) respectively define the sawtooth serration profile $\zeta^{(s)}(y_2)$ and the slit serration profile $\zeta^{(l)}(y_2)$.

$$y_1 = \zeta^{(s)}(y_2) = \begin{cases} (4h_s/\lambda_s)(y_2 - n\lambda_s), & n\lambda_s < y_2 < (n+\tfrac{1}{2})\lambda_s \\ -(4h_s/\lambda_s)(y_2 - n\lambda_s), & (n-\tfrac{1}{2})\lambda_s < y_2 < n\lambda_s \end{cases}, \quad n = 0, \pm 1, \pm 2, \pm 3, \ldots, \tag{1}$$

$$y_1 = \zeta^{(l)}(y_2) = \begin{cases} -h_1, & n(d_1+d_2) < y_2 < (n+1)d_1 + nd_2 \\ h_1, & (n+1)d_1 + nd_2 < y_2 < (n+1)(d_1+d_2) \end{cases}, \quad n = 0, \pm 1, \pm 2, \pm 3, \ldots, \tag{2}$$

where $2h_S$ and $2h_l$ are their respective root-to-tip distances, and λ_S and d_1+d_2 are their respective spatial periodicity.

Using the appropriate Green's function $G(\mathbf{x},\mathbf{y};\omega)$ that satisfies the Kutta condition at the trailing edge, and by means of integration over the surface of the flat plate model (in the region $y_2 \le 0$) the pressure in the region below the boundary layer sources $p(\mathbf{x};\omega)$ is given by Equation (3). Details of the derivation can be found in [2].

$$p(\mathbf{x};\omega) = \frac{i}{2}\int_{-\infty}^{\infty} dy_2 \int_{-\infty}^{\psi(y_3)} dy_1 \int_{-\infty}^{\infty} \gamma(K)\left[G(\mathbf{x},y_1,y_2;\omega)\right] \times p_s(\mathbf{K};\omega) e^{i[K_1 y_1 + K_2 y_2]} d^2\mathbf{K} \tag{3}$$

where $\boldsymbol{K}=(K_1,K_2,0)$ is the boundary layer turbulent wavenumber vector, $\gamma(K) = \sqrt{\kappa_0^2 - K^2}$, $\kappa_0 = \omega/c_0$ is the acoustic wavenumber and $p_S(\mathbf{K};\omega)$ is the wavenumber frequency spectrum of the boundary layer in the absence of the airfoil.

The acoustic pressure spectral density $\Phi(\mathbf{x},\omega)$ is given by $\left\langle p(\mathbf{x},\omega) p^*(\mathbf{x},\omega') \right\rangle = \Phi(\mathbf{x},\omega)\delta(\omega-\omega')$. For a finite section of the airfoil of length L wetted by the turbulent flow, the blocked surface wavenumber frequency spectral density $\Phi_S(K_1,K_2,\omega)$ is defined by

$$\left\langle p_s(K_1,K_2,\omega) p_s^*(K_1',K_2,\omega') \right\rangle \approx \frac{L}{2\pi}\Phi_S(K_1,K_2,\omega)\delta(K_1-K')\delta(\omega-\omega'), \tag{4}$$

where $-L/2 < y_2 < L/2$, and $L \gg \delta$. Finally, the wall pressure spectrum for the boundary layer pressure in the hydrodynamic region due to Chase [7] is given by:

$$\Phi_S(\mathbf{K},\omega) = \frac{C_m \rho^2 v_*^3 K_1^2 \delta^5}{[(K_1 - \omega/U_c)^2(\delta U_c/3v_*)^2 + (K\delta)^2 + \varepsilon^2]^{5/2}} \tag{5}$$

where δ is the turbulent boundary layer thickness at the trailing edge, $K = |\vec{K}|$, $v_* \approx 0.03U$ is the skin friction, $C_m \approx 0.1533$, $\varepsilon = 1.33$ are constants given by Howe [2] and the convection velocity is approximately $U_c \approx 0.7U$, where U is the mean flow velocity.

Noise prediction model for a straight edge

Before investigating the effect on noise of serrations, the noise radiation from a straight trailing edge is presented. This is readily achieved by putting $\zeta(y_2) = 0$ in the radiation integral of Equation (3). The integration over y_2 in this case is equal to $2\pi\delta(K_2)$, which suggests that, in this infinite span limit, only the turbulent wavenumber contribution $K_2 = 0$ (*i.e.* perpendicular to the trailing edge) radiates to the far field.

The far field pressure spectral density for a straight trailing edge $\Phi_0(\mathbf{x},\omega)$ can be deduced by combining Equation (3) and (4) and using the appropriate Green's function [2].

$$\Phi_0(\mathbf{x},\omega) \approx \frac{\omega L \sin(\psi)\sin^2(\theta/2)}{2\pi c_0 |\mathbf{x}|^2} \int_{-\infty}^{+\infty} \frac{\Phi_S(K_1,0;\omega)}{|K_1|} dK_1 \tag{6}$$

The integration over streamwise wavenumber K_1 can be simplified by noting from Equation (5) that the surface pressure spectral density $\Phi_S(\mathbf{x},\omega)$ is dominated by turbulent eddies, which convect close to the convection velocity U_c. Therefore, the wavenumber integral can be replaced with the value of the integrand at $K_1 = \omega/U_c, K_2 \approx 0$.

Noise prediction model for a serrated sawtooth edge

To predict the noise generation from a sawtooth serrated trailing edge, the trailing edge profile given by Equation (1), $y_1 = \zeta^{(s)}(y_2)$ is introduced in the radiation integral of Equation (3). The dual integration with respect to y_1 and y_2 can then be readily evaluated as follows. The spanwise integra-

tion over y_2 leads to an expression of the form $\Sigma \exp(jnK_2\lambda_s)$, taken over the whole span profile. This term can be re-written using the identity (Poisson sum):

$$\sum_{n=-\infty}^{+\infty} e^{jnK_2\lambda_S} = \frac{2\pi}{\lambda_S}\sum_{n=-\infty}^{+\infty}\delta\left(K_2 - \frac{2\pi n}{\lambda_S}\right) \tag{7}$$

Equation (7) suggests that only the discrete turbulent wavenumber $K_2 = 2\pi n/\lambda_s \quad (n = 0, \pm 1, \pm 2, \pm 3, \cdots)$ contributes to the far field noise. The streamwise integration, y_1 has to be treated as a generalized function, and is found to be equal to

$$\int_{-\infty}^{0} |y_1|^{1/2} e^{jK_1 y_1} dy_1 = -\frac{\sqrt{\pi}}{2} e^{j\pi/4} |K_1|^{-3/2} \tag{8}$$

Finally, the far field noise spectral density $\Phi(\mathbf{x},\omega)$ for a serrated trailing edge is given by:

$$\Phi(\mathbf{x},\omega) \approx \frac{2h_s^2 \omega L \sin\psi \sin^2(\theta/2)}{\pi c_0 |\mathbf{x}|^2} \sum_{n=-\infty}^{\infty} \int_{-\infty}^{+\infty} \left(1 - \frac{\cos(2K_1 h_s)}{\cos(n\pi)}\right) \times \frac{\left|K_1^2 + (2n\pi/\lambda_s)^2 - \kappa_0^2\right|}{(n^2\pi^2 - 4K_1^2 h_s^2)^2 |K_1|} \Phi_S(K_1, 2n\pi/\lambda_s) dK_1 \tag{9}$$

The integral over K_1 can be evaluated in a similar fashion as mentioned above for a straight edge, by restricting the integrand to $K_1 = \omega / U_c$.

Extension of Howe's trailing edge noise model to slitted geometries

Substituting Equation (2), $y_1 = \zeta^{(l)}(y_2)$, which defines the slit serration profile, into Equation (3), the spanwise integral over y_3 reveals that only the discrete wavenumbers, given in Equation (10), contribute to the far field noise spectrum $\Phi(\mathbf{x},\omega)$.

$$K_2 = \frac{2\pi n}{d_1 + d_2}, \quad n = 0, \pm 1, \pm 2, \pm 3, \cdots \tag{10}$$

The streamwise integral (y_1) is calculated using Equation (8) as before. The far field noise spectrum $\Phi(\mathbf{x},\omega)$ for a slit serration, given by Equation (11) is therefore:

$$\Phi(\mathbf{x},\omega) \approx \frac{8\omega L \sin\psi \sin^2(\theta/2)}{\pi c_0 |\mathbf{x}|^2} \times \sum_{n=-\infty}^{\infty} \int_{-\infty}^{\infty} \sin^2\left(n\pi \frac{d_1}{d_1 + d_2}\right) \sin^2\left(\tfrac{1}{2} K_1 h_l\right) \times \frac{\left|K_1^2 + 4n^2\pi^2/(d_1 + d_2)^2 - \kappa^2\right|}{n^2 |K_1|^3} \Phi_S\left(K_1, \frac{2\pi n}{d_1 + d_2}; \omega\right) dK_1 \tag{11}$$

As before the K_1 integral can be approximated by the value of the integrand at $K_1 = \omega / U_c$.

EXPERIMENTAL SETUP

As part of the European project FLOCON, a test campaign aimed at reducing trailing edge noise on a NACA6512 airfoil has been carried out in the ISVR's open-jet wind tunnel. The goal of this study was to reduce the broadband noise generated by turbulent boundary layers using passive treatments such as sawteeth and other trailing edge geometries. This section describes the setup and the airfoil model used for these experiments.

The facility

The ISVR open-jet wind tunnel described by Chong et-al [8] was used for studying trailing edge noise reduction on a NACA6512 airfoil. Air is supplied from a centrifugal fan driven by a variable speed 110 kW motor. The maximum flow velocity from the nozzle is $M \approx 0.4$. The dimensions of the nozzle exit are 0.45 m in width by 0.15 m in height. The jet at the nozzle exit plane has a turbulence intensity of 0.45 %. As seen in Figure 3, the nozzle is situated in the ISVR's large anechoic chamber of dimensions 8 x 8 x 8 m. The use of side plates mounted flush with the nozzle exit maintains the flow two dimensional and helps to support the test model horizontally.

Measurements of the far field noise are performed using a 19 B&K polar microphone array located at 1.2 m from the trailing edge (Figure 3). Microphones are placed at polar angles of between 45° and 135°. Noise data are recorded for the four mean flow velocities of 20, 40, 60 and 80 m/s and for the five geometrical angles of attack: -5, 0, 5, 10 and 15°. Note that due to jet deflection by the airfoil, the angle of attack correction given by Brooks et-al [9] was applied to convert the geometrical angles of attack α_g to effective angles of attack in free air α_e. The geometrical angle of attack α_g in the rig is defined as the angle between the flow and the chord line. Turbulence in the boundary layer is generated by the use of a rough trip band placed on both suction and pressure sides of the airfoil, downstream of the leadisng edge, from 10% to 15% of the airfoil chord.

Unless stated otherwise, all noise data presented in this paper are measured at 90° overhead of the trailing edge, at 5° angle of attack and a flow speed of 40 m/s.

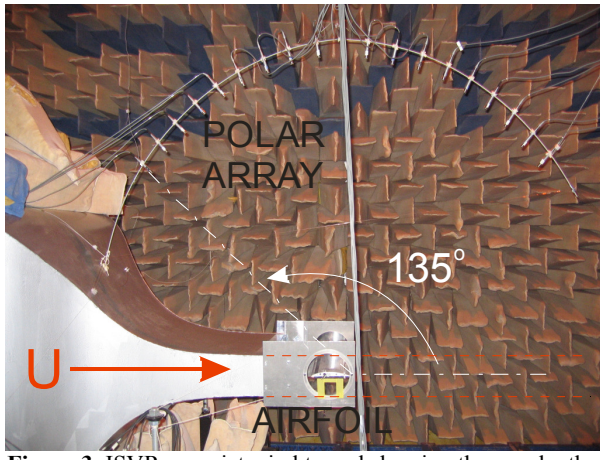

Figure 3. ISVR open-jet wind tunnel showing the nozzle, the airfoil model and the polar array in the anechoic chamber

Airfoil model

The airfoil model used for the study of trailing edge noise reduction is a NACA6512-10 cambered profile with 0.16 m chord and 0.45 m span. It is a high lift device used in turbomachinery and wind turbine applications. The airfoil has been designed and manufactured as part of the European project FLOCON as a baseline model for the investigation of trailing and leading edge noise reduction treatments. Figure 4 shows a picture of the airfoil in the rig and fitted with a sawtooth trailing edge.

The test airfoil is composed of a main steel body of 0.1 m in length and a detachable trailing edge, 0.06 m in length, which allows flat plate geometries to be inserted at the airfoil trailing edge. Capillary tubes of 0.6 mm external diameter are connected to the surface in the mid-span plane and run along the span of the airfoil allowing measurements of the static and unsteady pressure to be taken for all trailing edge geometries. As shown in Figure 4 trailing edge serrations are cut into thin flat plates and inserted into the airfoil. All inserts are made of rigid cardboard of thickness 0.8 mm, which were cut with a laser to ensure precision. This process of attachment avoids any bluntness at the root of the serrations that result in vortex shedding and introduce strong tones in the far field noise spectra. A straight unserrated edge made of the same material is used as the baseline configuration for all tests.

Figure 4. Picture of the NACA6512 airfoil in situ with serration $\lambda_S/h_S = 0.6$

Five sawtooth and four slitted trailing edge serrations were tested. Their geometry is given in Table 1 in terms of root-to-tip distance h_S and h_I and spatial periodicity λ_S and $d_1 + d_2$, for the sawtooth and slitted serrations, as shown in Figures 1 and 2.

Table 1. Geometry of the sawtooth and slit serration flat plate inserts

Sawtooth serrations			Slit serrations			
λ_S	h_S	λ_S/h_S	d_1	d_2	h_I	$(d_1+d_2)/h_I$
1.5	15	0.1	0.5	0.5	15	0.067
1.5	10	0.15	0.5	1	15	0.1
3	15	0.2	1	1	15	0.133
3	10	0.3	1	1	10	0.2
9	15	0.6	-	-	-	-

Static pressure distribution

The static pressure coefficient distribution along the airfoil chord was measured for each serration at 60 m/s and at each angle of attack α_g mentioned previously. It was measured at 10 locations on both pressure and suction sides of the airfoil using a Furness FC014 micro manometer coupled to a scanivalve unit that allows a rapid measurement of the static pressure along the chord using a single pressure manometer. The distribution of the static pressure coefficient C_p defined in Equation (12) is used to quantify the influence of the various trailing edge serrations on the sectional lift.

$$C_p = \frac{P_i - P_\infty}{\frac{1}{2}\rho U^2} \qquad (12)$$

where P_i is the static pressure measured at location i along the airfoil chord, P_∞ is the atmospheric pressure, ρ the air density and U the mean flow velocity. Figure 5 shows a comparison of the static pressure coefficient distribution C_p along the airfoil chord between the measured sharp edge airfoil, the RANS prediction, and a number of measured sawtooth and slit serrations, at $\alpha_g = 5^o$ angle of attack. No significant influence on the steady loading around the airfoil by the serrations can be seen. Note that as the airfoil is fitted with a detachable trailing edge, there is no static pressure sensor close to the trailing edge. Thus the effect of the serrated edges in this trailing edge region could not be estimated. However, as most of the lift is generated on the upstream part of the airfoil, it is reasonable to assume that the introduction of trailing edge serrations cause negligible reductions in lift.

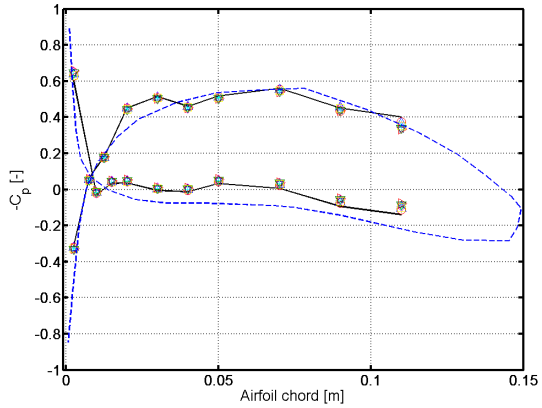

Figure 5. Static pressure distribution coefficient Cp at $\alpha_g = 5^o$ (Solid) measured baseline, (Dashed) baseline Turb'Flow RANS CFD by Fluorem, (Symbols) Sawtooth and slit serrations defined in Table 1

THEORETICAL NOISE REDUCTION

The theoretical expressions of Equations (9) and (10) are used to calculate the noise reduction ΔSPL as given by Equation (13).

$$\Delta SPL = 10 \cdot \log_{10}\left(\frac{\Phi_0(\mathbf{x},\omega)}{\Phi(\mathbf{x},\omega)}\right), \qquad (13)$$

where $\Phi_0(\mathbf{x},\omega)$ is the noise spectral density for the baseline straight edge airfoil, $\Phi(\mathbf{x},\omega)$ is the noise spectral density for the treated airfoil. Figures 6 and 7 present the predicted noise reduction ΔSPL for the sawtooth serrations and for slit serrations, for the parameters λ_S/h_S and $(d_1+d_2)/h_I$ given in Table 1. Experimental values of U and δ are used as input parameters to the models. Noise reductions are predicted at 90° overhead of the trailing edge, for a mean flow velocity $U = 40$ m/s and a measured turbulent boundary layer thickness of $\delta = 7.1$ *mm* for the straight edge and *8 mm* for the serrations (airfoil at 5° angle of attack).

Howe [2] shows that for sawtooth serrations, the highest level of noise reduction is achieved when $h_S > \delta$ and $\lambda_S > \delta$.

Strong oscillations can be seen in these figures due to interference between the root and the tip of the serrations for both sawtooth and slit serrations. The amplitude of these peaks in the noise reduction increases with decreasing values of λ_S/h_S and $(d_1+d_2)/h_I$. The frequency of these peaks is independent on the spatial periodicity of the serrations and is fixed by the condition $f = (n+\frac{1}{2})U/(4h_S)$ for the sawtooth profiles and $f = nU/h_I$ for the slit serrations.

Figure 6 shows that the noise reduction defined by Equation (13) increases with frequency and as shown by Howe [2], asymptotes to $10.log_{10}(1+(4h_S/\lambda_S)^2)$ for $\omega h_S/U_c >> 1$. It suggests that the sharper the sawtooth ($\lambda_S/h_S << 1$) the higher the noise reduction, especially at high frequencies. Figure 7 shows that the noise reduction, defined by Equation (13), decreases with frequency and asymptotes to zero for the slit serrations.

Figure 7 suggests that the slit serrations are not an effective noise reduction treatment since the noise reduction asymptotes to zero at high frequencies. These results also suggest that the introduction of obliqness of the edge relative to the flow direction by the sawtooth profiles is one of the reasons for the high noise reduction potential, at least in the high frequency region.

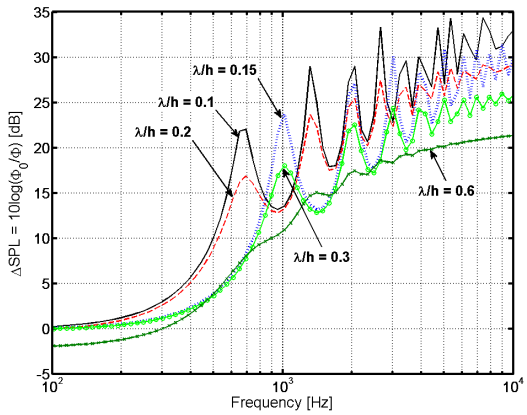

Figure 6. Predicted noise reduction for sawtooth serrations – Values λ/h as defined in Table 1

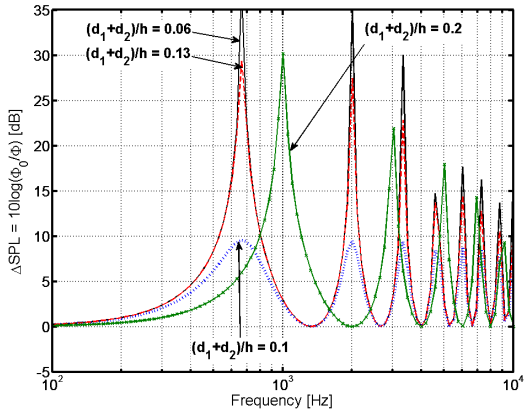

Figure 7. Predicted noise reduction for slit serrations – Values $(d_1+d_2)/h$ as defined in Table 1

EXPERIMENTAL RESULTS

Figures 8 to 12 show a comparison of the background-corrected far field noise PSD spectrum, measured at 90° overhead of the airfoil trailing edge, between the serrated (saw tooth and slit) and the sharp edge airfoil trailing edges, as defined in Table 1. Figures 8 and 9 present the data from 300 Hz to 7 kHz. Below 700 Hz, a noise reduction relative to the unserrated edge of between 3 to 5 dB can be seen for all trailing edge treatments. As previously reported in various experiments ([3, 4]) the noise model proposed by Howe (and the extended model presented above for slit serrations) over-predicts considerably the noise reduction achieved in practice. Various reasons for such differences are proposed by Gruber *et al* [6]. However, the trend in Howe's model is that the noise reduction increases as λ_S/h_S and $(d_1+d_2)/h_1$ reduces. Figure 8 shows that the greatest measured noise reduction is obtained for $\lambda_S/h_S = 0.3$ (≈ 5 dB) for the saw tooth trailing edges. In addition, while Howe's model predicts that the noise reduction increases as λ_S/h_S decreases, Figure 8 shows that the greatest noise reduction is obtained for the two sawtooth serrations with smallest h_S, which contradicts Howe's prediction. Figure 9 shows that the greatest noise reduction is ~1 dB obtained for $(d_1+d_2)/h_1 = 0.1$ for the slit trailing edges. Figure 8 also shows that all sawtooth trailing edges give a noise reduction from 300 Hz to 7 kHz while, as seen in Figure 9, the slit serrations increase the noise by 1 to 2 dB in this frequency range.

Oerlemans *et al* [4] have observed experimentally that trailing edge sawtooth serrations tend to increase the noise at high frequencies, which he attributed to non-alignement of the serrations with the flow direction. In practice, as the angle of attack of the airfoil is changed a misalignement of the trailing edge serrations with the flow occurs. Figures 10 and 11 show the high frequency content of the noise spectra presented Figures 8 and 9, from 7 to 20 kHz. It can be seen that serrated trailing edges increase the noise at high frequencies by 1 to 5 dB. For the noise spectra related to the saw tooth shown in Figure 10, the noise levels seem to be strongly dependent on h_S. When h_S is small, the noise is increased by 1 to 2 dB relative to the baseline in this frequentcy range. When h_S increases, howver, the noise is increased by 4 to 5 dB relative to the baseline. Figure 11 shows the same phenomon for the slit profiles where d_1 and d_2 are now the appropriate parameters. When $d_1 = d_2$, the noise is increased by 1 to 2 dB while for $d_1 \neq d_2$ the noise is increased by 3 dB relative relative to the baseline in the frequency range 7 to 20 kHz .

As demonstrated by Amiet [10], Brooks [9] and Howe [11, 1, 2], trailing edge noise consists of two main noise generation mechanisms that radiate to the far field, direct radiation from the incident pressure in the turbulent boundary layer and the radiation from the scattered incident pressure in the turbulent boundary layer at the trailing edge. The mathematical model presented in Section 1 assumes that the scattering process is the main noise generation mechanism. Experimental data confirms that it is one of the main mechanisms since noise reductions of up to 5 dB relative to the baseline are achieved by the introduction of such geometries at the trailing edge. However, it also suggests that other noise generation mechanisms are involved since the predicted attenuations are significantly greater than the ones obtained experimentally.

Figures 12 and 13 show the variation of the noise reduction ΔSPL defined by Equation (13) versus frequency and mean flow velocity U for the saw tooth serration $\lambda_S/h_S = 0.1$ and the slit serration $(d_{1+}\, d_2)/h_1 = 0.067$. Distinct region of noise increase and reduction can be seen with the separation between these two regions closely matching the line Equation (14).

$$St_0 = \frac{f_0 \delta}{U - U_0} \approx 1.18 \qquad (14)$$

where f_0 is the critical frequency above which noise is increased and $U_0 = 0$. U_0 is a constant velocity convection used to take into account the fact that the Strouhal number St_0 does not appear to pass through the origin. The precise behaviour of St_0 for $f \to 0$ cannot be deduced from this data owing to poor signal to noise ratio at low jet velocities. Note that f_0 must go to zero as $U \to 0$. Note that values of $St = 1.18$ are reasonably constant for all serration geometries.

Figure 13 also shows that the lower frequency band within which noise is increased can be delimited by Equation (14)

for the following values $St_0 = 0.71$, $U_0 = 10$ *m/s* and $St_0 = 0.14$, $U_0 = 5$ *m/s*. The value of U_0 increases with decreasing Strouhal number, but does not show any particular dependence on physical parameters such as the geometry of the serrations λ_S/h_S. Detailed measurements on each of the serrated edges would probably provide the correct value for δ and nullify U_0.

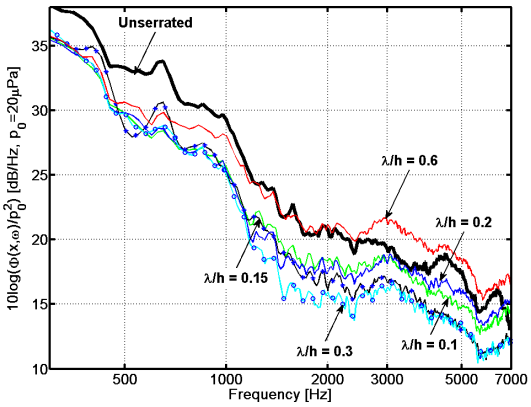

Figure 8. Background corrected far field acoustic spectrum showing a comparison between the unserrated edge and the sawtooth serrations.

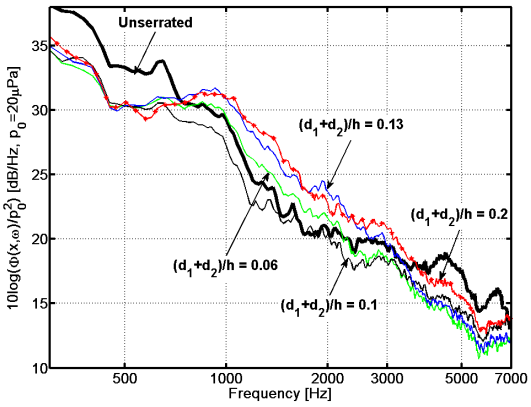

Figure 9. Background corrected far field acoustic spectrum showing a comparison between the unserrated edge and the slit serrations.

Figures 14 and 15 show the variation of the Strouhal number St_0 and U_0 (respectively) with increasing values of λ_S/h_S for the sawtooth serrations and $(d_1+d_2)/h_1$ for the slit serrations. For the sawtooth edges, both St_0 and U_0 seem to slightly increase with increasing λ_S/h_S while both St_0 and U_0 are reasonably constant for the slit serrations $(d_1+d_2)/h_1$. It therefore seems that Equation (14) provides a good estimation of the critical frequencies f_0 that delimitate the areas of noise increase and reduction in Figures 12 and 13, and Figures 16 to 22 in the Appendix.

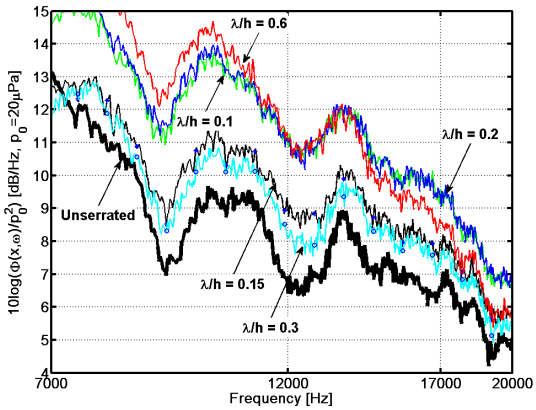

Figure 10. Background corrected far field acoustic spectrum showing a comparison between the unserrated edge and the slit serrations at high frequencies.

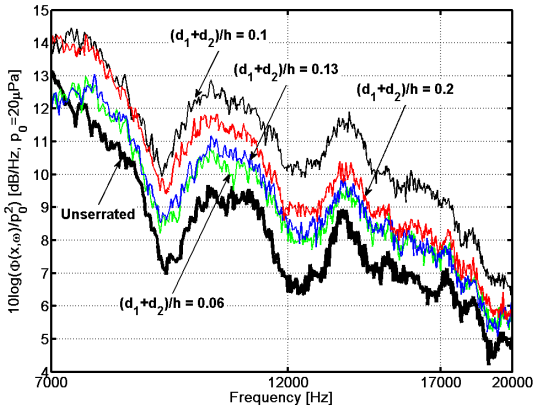

Figure 11. Background corrected far field acoustic spectrum showing a comparison between the unserrated edge and the slit serrations at high frequencies.

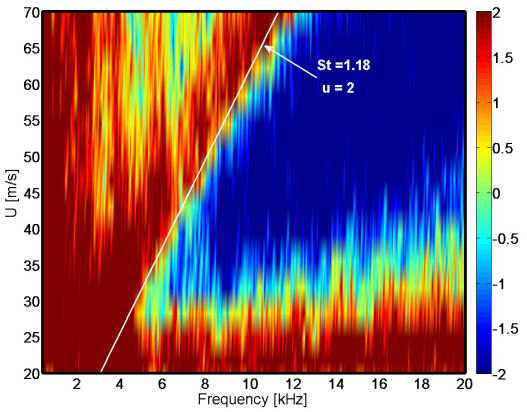

Figure 12. Noise reduction ΔSPL (Equation (13)) in dB as a function of U and frequency – Sawtooth $\lambda_S/h_S = 0.1$.

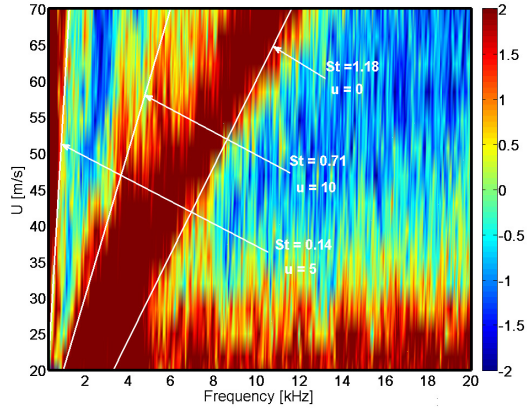

Figure 13. Noise reduction ΔSPL (Equation (13)) in dB as a function of U and frequency - Slit $(d_1+d_2)/h_1 = 0.067$.

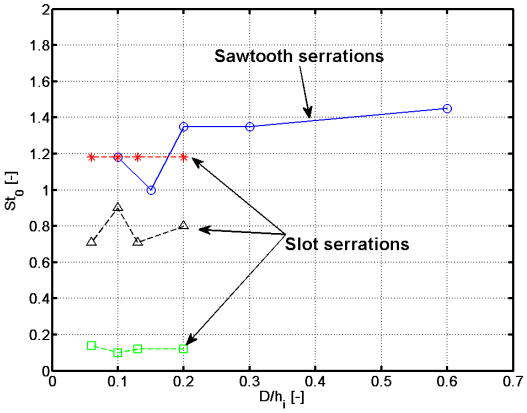

Figure 14. Variation of St_0 (Equation (14)) as a function of D/h_i where $D = \lambda_S$, $h_i = h_S$ for the sawtooth serrations and $D = (d_1+d_2)$, $h_i = h_1$ for the slit serrations

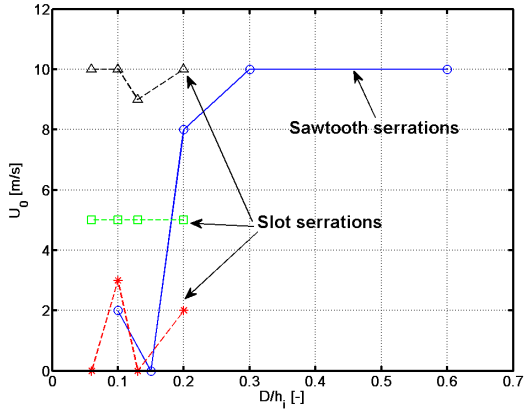

Figure 15. Variation of U_0 (Equation (14)) as a function of D/h_i where $D = \lambda_S$, $h_i = h_S$ for the sawtooth serrations and $D = (d_1+d_2)$, $h_i = h_1$ for the slit serrations

CONCLUSION

Following Howe's ideas on the prediction of far field noise radiation from a serrated trailing egde [1, 2], a similar expression for the scattered pressure is derivated for a slit serration. Predictions from the sawtooth and slit serrations show a potential noise reduction of about 30 to 35 dB at high frequencies. For sawtooth serrations, frequencies at which peaks in noise reduction appear are fixed by h_S while the amplitude increases with h_S/λ_S. For slit serrations, frequencies at which peaks in noise reduction appear are fixed by h_1 while the amplitude increases when $d_1 = d_2$ and d_1 is small.

In practice, experimental data show that sawtooth serrations reduce noise efficiently by about 5 dB in the low to mid frequency ranges while slit serrations reduce noise by about 3 at low frequencies but increase the noise from about 700 Hz. A common high frequency noise increase has been found for all geometries. The critical frequencies f_0 above which noise is increased vary with mean flow velocity and follow the relation based on the Strouhal numbers $St_0 = f_0\delta / (U - U_0)$, and $St_0 \approx 1.18$, where U_0 is the value of U when $U \to U_0$. The increase of noise for the slit serrations at mid frequencies has been shown to follow the same relations for different Strouhal numbers values. In addition, each frequency region of noise increase can be well limited by one critical frequency for which the Strouhal number is constant.

Finally, this paper suggests that the mechanisms by which serrated trailing edges reduce the radiated noise are not yet fully understood. Indeed, Howe's theory assumes that the scattering process in the generation of airfoil trailing edge noise is the predominant noise source. This paper proves that such reductions cannot be achieved and suggests that other mechanisms of noise generation are also involved and dominant.

APPENDIX

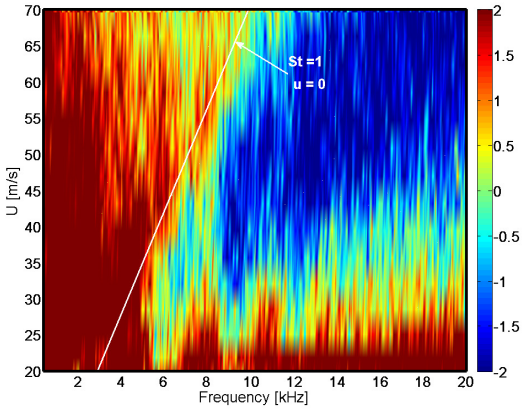

Figure 16. Noise reduction ΔSPL (Equation (13)) in dB as a function of U and frequency – Sawtooth $\lambda_S/h_S = 0.15$.

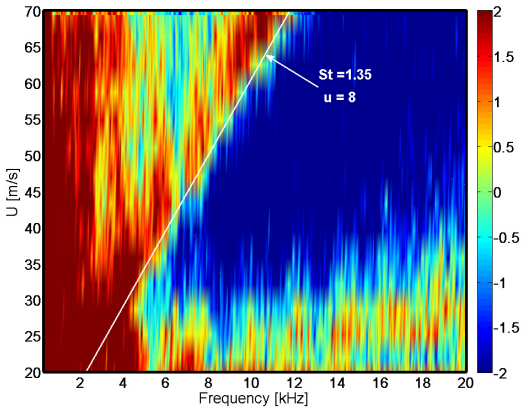

Figure 17. Noise reduction ΔSPL (Equation (13)) in dB as a function of U and frequency – Sawtooth $\lambda_S/h_S = 0.2$.

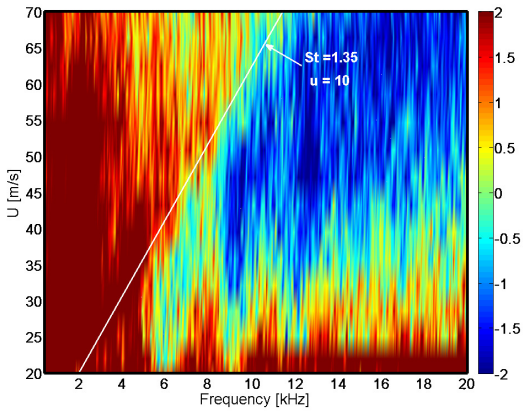

Figure 18. Noise reduction ΔSPL (Equation (13)) in dB as a function of U and frequency – Sawtooth $\lambda_S/h_S = 0.3$.

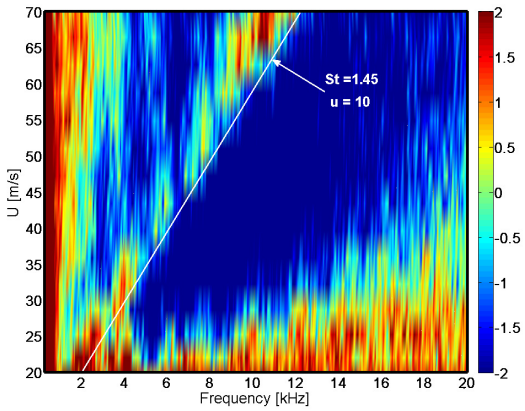

Figure 19. Noise reduction ΔSPL (Equation (13)) in dB as a function of U and frequency – Sawtooth $\lambda_S/h_S = 0.6$.

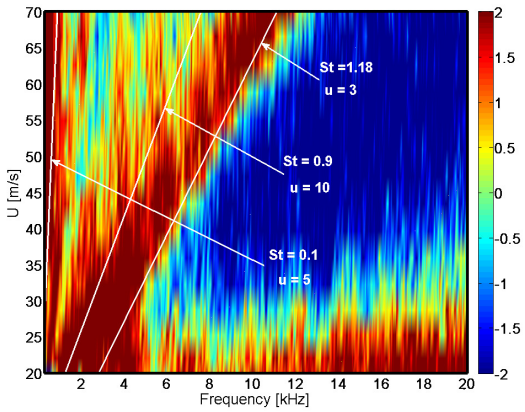

Figure 20. Noise reduction ΔSPL (Equation (13)) in dB as a function of U and frequency - Slit $(d_1+d_2)/h_l = 0.1$.

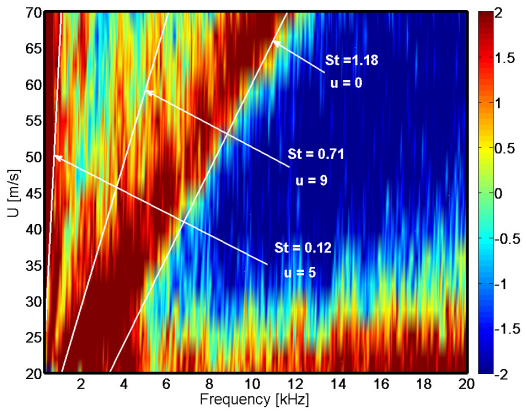

Figure 21. Noise reduction ΔSPL (Equation (13)) in dB as a function of U and frequency - Slit $(d_1+d_2)/h_l = 0.13$.

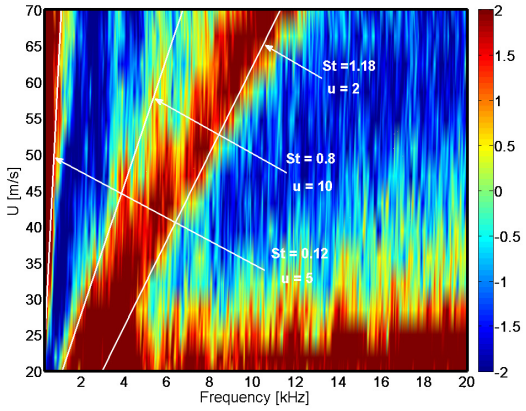

Figure 22. Noise reduction ΔSPL (Equation (13)) in dB as a function of U and frequency - Slit $(d_1+d_2)/h_l = 0.2$.

ACKNOWLEDGMENTS

This work was supported by the 7TH Framework European Project FLOCON: Adaptive and Passive Flow Control for Fan Broadband Noise Reduction.

REFERENCES

[1] MS Howe. Aerodynamic noise of a serrated trailing edge. *Journal of Fluids and Structures*, 5(1), pp. 33–45, 1991.

[2] MS Howe. Noise produced by a sawtooth trailing edge. *The Journal of the Acoustical Society of America*, 90, pp. 482, 1991.

[3] AGM Dassen, R. Parchen, J. Bruggeman, and F. Hagg. Results of a wind tunnel study on the reduction of airfoil self-noise by the application of serrated blade trailing edges. In *Proc. of the European Union Wind Energy Conference and Exhibition, Göteborg*, pp. 800–803, 1996.

[4] S. Oerlemans, M. Fisher, T. Maeder, and K. Kögler. Reduction of wind turbine noise using optimized airfoils and trailing-edge serrations. *AIAA journal*, 47, pp. 1470–1481, 2009.

[5] R. Parchen, W. Hoffmans, A. Gordner, and K. Braun. Reduction of airfoil self-noise at low Mach number with a serrated trailing edge. In *International Congress on Sound and Vibration, 6 th, Technical Univ. of Denmark, Lyngby, Denmark*, pp. 3433–3440, 1999.

[6] M. Gruber, P. Joseph, and TP. Chong. Experimental investigation of airfoil self noise and turbulent wake reduction by the use of trailing edge serrations. In *16th AIAA/CEAS Aeroacoustics Conference*, 2010.

[7] DM Chase. The character of the turbulent wall pressure spectrum at subconvective wavenumbers and a suggested comprehensive model. *Journal of Sound and Vibration*, 112(1), pp. 125–147, 1987.

[8] TP Chong, PF Joseph, and P. Davies. Design and performance of an open jet wind tunnel for aero-acoustic measurement. *Applied Acoustics*, 70(4), pp. 605–614, 2009.

[9] TF Brooks and TH Hodgson. Trailing edge noise prediction from measured surface pressures. *Journal of Sound Vibration*, 78, pp. 69–117, 1981.

[10] RK Amiet. Noise due to turbulent flow past a trailing edge. *Journal of Sound and Vibration*, 47(3), pp. 387–393, 1976.

[11] MS Howe. Trailing edge noise at low Mach numbers. *Journal of Sound and Vibration*, 225(2), pp. 211–238, 1999.